A multi-instrument measurement of a mesospheric bore at the equator

K. Shiokawa, S. Suzuki, Y. Otsuka, and T. Ogawa

Solar-Terrestrial Environment Laboratory, Nagoya University, Toyokawa, Japan

T. Nakamura

Research Institute for Sustainable Humanosphere, Kyoto University, Uji, Japan.

M. G. Mlynczak

Climate Science Branch, NASA Langley Research Center, Hampton, Virginia, U.S.A.

J. M. Russell III

Department of Physics, Hampton University, Hampton, VA 23668, U.S.A.

To be submitted to Journal of the Meteorological Society of Japan (JMSJ) (http://www.jstage.jst.go.jp/browse/jmsj/-char/en) for the special issue of the CPEA project, deadline of submission: October 31, 2005.

T. Ogawa, T. Otsuka, and K. Shiokawa, Solar-Terrestrial Environment Laboratory, Nagoya University, Toyokawa 442-8507, Japan. (ogawa@stelab.nagoya-u.ac.jp; otsuka@stelab.nagoya-

Abstract. We have made a comprehensive measurement of mesospheric bore phenomenon at the equator at Kototabang, Indonesia (0.2°S, 100.3°E), using an airglow imager, an airglow temperature photometer, a meteor radar, and the SABER instrument on board the TIMED satellite. The bore was detected in airglow images of both OH-band (peak emission altitude: 87 km) and 557.7-nm (96 km) emissions, as east-west front-like structure propagating northward with a velocity of 52-58 m/s. Wave trains with a horizontal wavelength of 30-70 km are observed behind the bore front. The airglow intensity decreases for all the mesospheric emissions of OI (557.7 nm), OH-band, O_2-band (altitude: 94 km), and Na (589.3 nm) (90 km) after the bore passage. The rotational temperatures of both OH-band and O_2-band also decrease ∼10 K after the bore passage. An intense shear in northward wind velocity of 80m/s was observed at altitudes of 84-90 km by the meteor radar. Kinetic temperature profile at altitudes of 20-120 km was observed near Ko-

u.ac.jp; shiokawa@stelab.nagoya-u.ac.jp)

T. Nakamura, Research Institute for Sustainable Humanosphere, Kyoto University, Gokanosho, Uji, Kyoto 611-0011, Japan. (nakamura@rish.kyoto-u.ac.jp)

M. G. Mlynczak, Climate Science Branch, NASA Langley Research Center, 21 Langley Blvd., Mail Stop 420, Hampton, VA 23681-0001, USA. (m.g.mlynczak@nasa.gov)

James M. Russell III, Department of Physics, Hampton University, Hampton, VA 23668, U.S.A. (james.russell@hamptonu.edu)

totabang by TIMED/SABER. On the basis of these observations, we discuss generation and ducting of the observed mesospheric bore.

Japanese Abstrast:

この論文では、２００４年８月５日の夜間にインドネシア・コトタバン (0.2°S, 100.3°E) で観測された中間圏の tidal bore（潮津波）を、大気光全天イメージャー、分光温度フォトメータ、流星レーダー、TIMED 衛星 SABER によって総合的に観測した結果を報告する。このような中間圏の bore は、高度 80-100km で夜間にごくわずかに発光する大気光の画像中で、津波のように伝搬する構造として、Taylor et al.[1995] によって最初に報告された。しかし、その総合的な観測の例はこれまで数例しかなく、赤道域での総合観測はこれが初めてである。この中間圏の bore は、この高度に存在する温度逆転層の中をダクト伝搬している、と Dewan and Picard [1998] により理論的に予想され、これまでの総合観測の例もそれを示していた。一方、今回の観測で得られた bore 発生時の温度、風速の高度プロファイルは、温度逆転層によるダクト伝搬を支持しておらず、同時に観測された中間圏風速の強い鉛直シアーが bore の生成に寄与しているのではないか、と考えている。

1. Introduction

The airglow imaging technique has been widely used since 1990s in accordance with the development of highly sensitive cooled-CCD image detector. It visualizes gravity waves in the mesopause region through the airglow emission. One of the most distinct structures seen in the mesospheric airglow images are tidal bore, which often represents front-like structure with following small-scale waves. *Taylor et al.* [1995] firstly reported a spectacular front-like structure with gravity waves behind, in the mesospheric airglow images at OI (557.7nm, (peak emission altitude: ∼96 km), OH-band (near infrared, ∼87 km), Na (589.3 nm, ∼90 km), and O_2 (near infrared, ∼94 km) observed at Haleakala, Hawai during the ALOHA-93 campaign. *Dewan and Picard* [1998] explained this front-like structure by internal mesospheric undular bore with a simple two-layer model constructed by analogy with the theory of bores in river channels. *Dewan and Picard* [2001] further discuss the origin of the bores in the mesosphere in the channel of already-existing inversion layer in the mesosphere. *Smith et al.* [2003] reported such temperature inversion layer from a sodium lidar measurement during a distinct (visible in naked eye) bore event in the southwestern United States. *She et al.* [2004] further reported a comprehensive measurement of an undular bore event in Colorado, using an OH airglow imager and a sodium temperature/wind lidar. They confirmed existence of a collocated temperature inversion layer to serve as the ducting region for bore propagation. *Fechine et al.* [2005] reported 64 mesospheric bore events based on two years of airglow imaging observations at Cariri, Brazil, (7.5°S, 36.5°W), indicating that the mesospheric bore is not a rare phenomenon.

Despite these previous measurements, it is still very rate to have comprehensive measurement of mesospheric bore using multi instruments. In this paper, we report a clear bore event observed at geographic equator using an airglow imager, an airglow temperature photometer, a meteor radar, and a satellite radiometer. It seems that the ducting channel of the bore by temperature inversion layer is not well developed for the present case. We suggest that vertical wind shear in the mesopause region may play an important role for generation of the undular bore.

2. Observation

2.1. Overview of airglow observations

An airglow imager and an airglow temperature photometer were installed at Kototabang, Indonesia (0.2°S, 100.3°E, dipole geomagnetic latitude (MLAT): −10.4°), on October 26, 2002, and February 28, 2004, respectively, as components for the CPEA (Coupling Processes in the Equatorial Atmosphere) project. They are part of the Optical Mesosphere Thermosphere Imagers (OMTIs) [*Shiokawa et al.,* 1999; 2000]. Both instruments use a thinned and back-illuminated cooled charge-coupled device (CCD) with 512 × 512 pixels. Airglow images at a wavelength of 557.7 nm (OI) and near-infrared OH-bands were obtained every 4.5 min with an exposure time of 105 s and 15 s, respectively. The airglow temperature photometer measures zenith airglow intensities and rotational temperatures of OH(6,2) P branch and O_2b (0,1) bands together with the airglow intensities at wavelengths of 557.7 nm (OI), 630.0 nm (OI), 777.4 nm (OI), 589.3 nm (Na) with a time resolution of 5.5 min at a zenith angle less than 14.7°. Figure 1 shows the occurrence rate of clear sky during the 2.6 years of the automated measurements by the airglow imager, from October 26, 2002, to June 12, 2005. Because of the tropical climate and surrounding

Figure 1

mountains of Sumatra Island, the sky at Kototabang tends to be cloudy. Chance of clear sky has a peak in May and June. For other months, the occurrence rate of clear sky is mostly less than 10%. However, because of long-term automated measurements, we have tens of hours of clear sky intervals for each month, as shown in the bottom of the panel. Several events of mesospheric bore were observed by the airglow imager in these clear-sky intervals. The event presented here is a distinct one during which other datasets from the photometer, radar, and satellite were also available.

2.2. Airglow imager

Figure 2 shows all-sky airglow images at OH-band (top) and OI (557.7nm) (bottom) at 1258–1402 UT (1958–2102 LT) on August 5, 2004, at Kototabang, Indonesia. The bright band from northeast to south in the bottom half of the images is the Milky Way (Galaxy). A front-like east-west structure moving northward can be recognized in both emissions. The airglow intensity decreases after the front-like structure passed. A gravity wave train with east-west phase front follows the front-like structure. These features are fairly consistent to the features of mesospheric undular bores reported in the previous papers [e.g., *Taylor et al.*, 1995; *Smith et al.*, 2003; *She et al.*, 2004; *Fechine et al.*, 2005].

Figure 2

To see the bore structure more clearly, we converted the all-sky images to geographic coordinates of (latitude, longitude) and calculated deviations in % from a 1.5 hour average image of 1244-1414 UT. The result is shown in Figure 3. The bore structure becomes more distinct. The gravity waves behind the bore has wavelengths of ∼30 km at (−1.2°–−1.7°N, 100.3°–101.1°E) in the OH-band image at 1332 UT, and ∼70 km at (−0.7°–−1.7°N, 100.3°–101.1°E) in the 557.7-nm image at 1358 UT. The front-like structure of the bore itself also has a north-south scale size of 30-70 km.

Figure 3

Figure 4 shows north-south cross sections (keograms) of the geographic airglow images of Figure 3. The cross sections are taken at longitudes of Kototabang (100.3°E). The northward-moving bore can be seen in both keograms. The northward velocities of the bore in the OH-band and 557.7-nm keograms are estimated to be 52 m/s and 58 m/s, respectively. The intensity of 557.7-nm emission drastically increases at ∼1310 UT. This increase is probably because of 557.7-nm emission from the thermosphere, as described below.

Figure 4

2.3. Airglow temperature photometer

During this event, the airglow temperature photometer measured intensities and rotational temperatures of several airglow lines at Kototabang, as shown in Figure 5. The photometer measured OH and O_2 rotational temperatures using each two filters with identical specifications. However, data from one OH filter has a problem of spectral fitting, and thus, data from only one filter is shown for the OH rotational temperature. As shown in Figures 2-4, the mesospheric bore crossed the zenith of Kototabang at ∼1330 UT. The rotational temperatures of OH and O_2 decreases ∼10 K after the passage of the bore at 1325–1350 UT. They seem to increase ∼5 K with approaching the bore front at 1300-1325 UT. The airglow intensities of OH, O_2, Na also increase and then decreases at the bore passage with amplitudes of 5-20 R.

Figure 5

The 557.7-nm emission increases at 1240–1330 UT, almost flat at 1330-1420 UT, and decreases after 1420 UT. These variations are quite similar to that of 630.0-nm emission. These variations in 630.0-nm emission correspond to the equatorial ionospheric anomaly, which is the enhanced 630-nm airglow band, moving to the geomagnetic equator (∼10° north of Kototabang) as the time goes from evening to midnight [e.g., *Shiokawa et al.*,

2005]. Because the 557.7-nm emission near the equator has a contribution from the thermosphere with ∼10-20 % of the 630.0-nm intensity, the variations in 557.7-nm emission are strongly affected by this anomaly motion. Nevertheless, a slight decrease of ∼10 R was observed at 1325–1340 UT, when the bore passed zenith of Kototabang.

2.4. Meteor radar

In order to see the background wind pattern during the bore event, we plotted mesospheric wind data obtained by a meteor radar collocated at Kototabang. The radar measures wind velocities at altitudes of ∼80–100 km through the Doppler shift of meteor echoes with a time resolution of 1 hour. Figure 6 indicates three-day variations in eastward and northward wind measured by the meteor radar on August 5-7, 2004. There are clear tidal variations with downward phase progression in both eastward and northward wind. It seems that a two-day variation is embedded on the tidal activity. For example, the northward winds at 1200–2400 UT on August 5 and 7 are stronger than that on August 6. As a result of these longer-time scale activities, the meridional wind is most intense and is larger than the zonal wind around the time of the bore event indicated by the arrows.

Figure 6

Figure 7 shows the eastward and northward wind profiles in the mesosphere at three time intervals (1130-1229UT, 1230-1329UT, and 1330-1429UT) around the bore event of August 5, 2004. The bore was around the zenith of Kototabang at ∼1330 UT. The wind profiles at 1230–1329 UT and 1330–1429 UT are mostly similar, and show intense northward wind of 48 m/s at 90 km and southward wind of >30 m/s below 84 km. An intense wind shear of 80 m/s/6km occurs in the northward wind between these altitudes. The northward wind velocity of 48 m/s at 90 km is comparable to the northward propagation velocity of the bore (52-58 m/s).

Figure 7

2.5. Satellite temperature profile

The other important parameter that determines propagation of gravity wave is the temperature. During the bore event, the Thermosphere Ionosphere Mesosphere Energetics and Dynamics (TIMED) satellite passed very close to Kototabang (101°E at 1348 UT at an altitude of 622 km) from southern to northern hemispheres. It measured height profile of kinetic temperature through the infrared emission from carbon dioxide in the Earth's limb, using the Sounding of the Atmosphere using Broadband Emission Radiometry (SABER) instrument [*Mertens et al.* 2001].

Figure 8 shows the height profile of the kinetic temperature measured by SABER on board the TIMED satellite at 1348 UT on August 5, 2004, at (3°S, 123°E) (∼2500 km east of Kototabang). The temperature has a maximum at 55 km and a minimum at 92 km. There is a temperature inversion layer at 74–81km, just below the airglow emission altitudes. The temperature simply increases above 92 km toward the thermosphere.

Figure 8

3. Discussion

We have made a comprehensive measurement of a mesospheric undular bore using ground-based and satellite instruments. The horizontal wavelength of the bore and waves behind were 30-70 km. The bore propagated northward with a velocity of 52-58 m/s, which was comparable to the background wind velocity (48 m/s) measured by the meteor radar at an altitude of 90 km. An intense wind shear from northward to southward was observed below this altitude. The temperature profile was simultaneously obtained by the TIMED/SABER instrument.

According to the model of mesospheric tidal bore by *Dewan and Picard* [1998; 2001], temperature inversion layer in the mesosphere acts as a guiding channel of the bore. In

Figure 8, such an inversion layer was observed at altitudes of 67–82 km, which was at lower altitudes than the airglow layers (82-100 km). The mesopause temperature minimum at 92 km may act as an another temperature inversion layer in connection with the lower thermosphere above 92 km.

Figure 9 shows height profile of the square of the Brunt-Väisälä frequency N^2, which is calculated from the temperature profile in Figure 8 and the MSIS90 model density profile. The values of N^2 has two peaks at 73 km and 92 km, corresponding to the two temperature inversion layers. However, these peaks in N^2 is much smaller than that modeled by *Dewan and Picard* [1998; 2001] and observed by *Smith et al.* [2003] and *She et al* [2004]. **Figure 9**

According to the bore model by *Dewan and Picard* [1998], the parameters that determines charactersitics of the bore are expressed as,

$$\beta = (h_1 - h_0)/h_0 \tag{1}$$

$$u_0 = \sqrt{\frac{g' h_1 (h_1 + h_0)}{2h_0}} \tag{2}$$

$$\lambda_h = \frac{2\pi h_1}{3}\sqrt{\frac{2h_0}{h_1 - h_0}} \tag{3}$$

$$a = \frac{1}{\sqrt{3}}\frac{h_1(h_1 - h_0)}{h_0} \tag{4}$$

where β, u_0, λ_h, a are the normalized bore strength [*Lighthill*, 1978], fluid speed relative to the bore before the bore passage, horizontal wavelength, and amplitude, respectively. h_0 and h_1 are the depth of the duct channel before and after the bore passage, respectively. g' is the acceleration of gravity corrected for buoyancy, given as $g' = g\Delta\phi/\phi$, where $\Delta\phi$ is the change in potential temperature from h_0 to h_1. Schematic pictures of these parameters are given in Figure 7 of *Dewan and Picard* [1998] and Figure 1 of *Smith et al.* [2003].

If we take the peak of N^2 at 92 km in Figure 9 as a possible bore channel, the vertical scale of the channel ($2h_0$) may be considered as ∼20 km, which is very large compared to that of the previous bores in literatures. Then, equation (3) gives $h_1 = 13$ km for $\lambda_h = 70$ km, while there is no reasonable solution of equation (3) for $\lambda_h = 30$ km. By taking potential temperatures at 92±10 km (6.5×10^3 K at 82 km and 1.5×10^4 K at 102 km), the value of g' was estimated as $g' = 9.5 \times (1.5 \times 10^4 - 6.5 \times 10^3)/((1.5 \times 10^4 + 6.5 \times 10^3)/2)$ = 7.5 m/s^2. Using h_0=10 km, h_1=13 km, and g' = 7.5 m/s^2, equations (1), (2), and (4) gives β=0.3, u_0=11 m/s, and a=2.3 km.

For $\beta < 0.3$, the waves after the bore is stable, while for $\beta > 0.3$, the waves will break to generate turbulence (a foaming bore). The value of β=0.3 estimated for the present event is just at the boundary of these two conditions, and is comparable to those reported in previous references (β =0.1–0.3, see Table 1 of *She et al.* [2004] for parameters of four previous bore events). The amplitude a is very large compared to the previous bores (0.19–0.68 km).

Despite of the above estimation of bore parameters, it is still questionable whether the N^2 peak at 92 km associated with the mesopause temperature decrease can act as a ducting channel for the bore formation. To see the ducting situation, we estimated condition of gravity wave propagation using the linear dispersion relation of the gravity waves, which is given as:

$$m^2 = \frac{N^2}{(u-c)^2} - k^2 - \frac{1}{4H^2} \tag{5}$$

where m ($= 2\pi/\lambda_z$), u, c, k ($= 2\pi/\lambda_h$), and H are the vertical wavenumber, background wind velocity, observed wave phase velocity, horizontal wavenumber, and scale height, respectively. We estimate m^2 and the vertical wavelength λ_z of the observed waves for

the case of λ_h = 30 and 70 km. The background meridional wind u measured by the meteor radar at 1230-1329 UT (Figure 7) was used, while it was assumed to be zero below 80 km and above 96 km. Temperature profile of Figure 8 and the MSIS90 model was used to estimate N^2 and H.

The bore was observed both in the 557.7-nm and OH images, which have emission altitudes of 96 km and 87 km with thicknesses of 6-10 km [e.g., *Zhang and Shepherd*, 1999]. Thus, the bore should exist at these altitudes. At 90 km, the northward wind velocity (u) is 48 m/s, which is comparable to the phase velocity (c) of the bore and the following waves. As a result, the vertical wavelengths of these structures are estimated to be very small (less than a few kilometers), indicating that the bore and the following waves are near the critical level condition.

Below 84 km, the background wind is southward of less than −30 m/s, as shown in Figure 7. Considering the horizontal wavelengths λ_h of 30 km and 70 km, the vertical wavelength of the waves become 92 km and 31 km at an altitude of 82 km, respectively. This suggests that the observed gravity waves with λ_h smaller than 30 km are nearly to be reflected by this opposite wind below the airglow layer, favorable to the ducting condition. However, the larger scale waves of ∼70 km can pass through this opposite wind layer.

Above 92 km the temperature increases toward the thermosphere. This temperature increase may set another reflection condition above the airglow layer, as suggested by the decrease in Brunt-Väisälä frequency N^2 in Figure 9. However, the estimated vertical wavelengths at 100-120 km are only 15–27 km for both λ_h =30 km and 70 km, indicating that waves with these horizontal scale can pass through the region of 92-120 km as freely propagating wave. From these considerations, the ducting condition proposed by *Dewan*

and Picard [1998] and observed by *Smith et al.* [2003] and *She et al.* [2004] seems to be not satisfied for the present bore event.

There are two points that should be considered for the above situation. One is that the temperature measurement by TIMED/SABER was done about 2500 km east of the observation point and may not represent the actual temperature profile above Kototabang. The temperature inversion layer at 65-80 km in Figure 8 is probably because of some large-scale waves, such as tides/planetary waves. If these waves have a horizontal scale of the order of 2500 km, the inversion layer may be at higher altitudes at Kototabang and contribute to the ducting of waves for the bore formation.

The other point is that intense shear of the meridional wind was observed at altitudes where the bore exists, as shown in Figure 8. Such shear was also reported during the bore event of *Smith et al.* [2003]. The direction of the shear is perpendicular to the bore front, and the propagation velocity of the bore is almost identical to the background wind velocity above the shear. This shear may contribute to the bore formation through K-H type instability, though theoretical approach would be needed to investigate such an idea.

4. Conclusion

A distinct bore was observed in the mesospheric airglow images at the equator at Kototabang, Indonesia (0.2°S, 100.3°E) at 1245–1415 UT (1945-2115 LT) on August 5, 2004. The observed features of the bore are summarized as:

1. The bore was observed in both OH-band (altitude: 87 km) and 557.7-nm (96 km) images. It propagates northward with velocities of 52 m/s in OH and 58 m/s in 557.7-nm images. Wave trains following the bore has horizontal wavelength of 30-70 km.

2. A zenith-looking photometer at Kototabang observed a slight increase and then a significant decrease in airglow intensities (at 557.7-nm, OH, O_2, and Na emissions) and rotational temperatures (OH and O_2, ∼10K) at the passage of the bore.

3. Northward wind measured by a meteor radar at Kototabang at 1230–1429 UT was 48 m/s at an altitude of 90 km, which is comparable to the northward velocity of the bore propagation. The wind was less than −30 m/s (southward) below 84 km, indicating an intense wind shear of 80 m/s/6km between 90 km and 84 km.

4. Mesospheric temperature profile measured by the TIMED/SABER instrument at ∼2500 km east of Kototabang at 1348 UT shows an temperature inversion layer at 74–81km, which is below the airglow emission altitudes. The mesopause was at 92 km.

On the basis of these observations, we estimated parameters of the tidal bore according to the model developed by *Dewan and Picard* [1998]. If we assume that the depth of the bore channel (h_0) to be 10 km by taking the mesopause at 92 km and a temperature increase above it as a temperature inversion layer, the model gives somewhat reasonable values of bore parameters (h_1=13 km, β=0.3, u_0=11 m/s, and a=2.3 km). However, considerations of gravity wave dispersion relation indicate that the observed mesopause structure was not sufficient to act as a ducting channel for the present bore. We suggest that the intense wind shear at 84–90 km may play an additional role for the bore generation.

Acknowledgments. We thank Y. Katoh, M. Satoh, and T. Katoh of the Solar-Terrestrial Environment Laboratory, Nagoya University, for their kind support of the development and operation of the all-sky imager and the photometer. The observation at Kototabang was carried out in collaboration with the Research Institute for Sustainable

Humanosphere (RISH), Kyoto University, Japan, and the National Institute of Aeronautical and Space Science (LAPAN), Indonesia. This work was supported by Grant-in-Aid for Scientific Research (13573006) and on Priority Area (764), and by the 21th Century COE Program (Dynamics of the Sun-Earth-Life Interactive System, No. G-4) of the Ministry of Education, Culture, Sports, Science and Technology of Japan.

References

Dewan, E. M., and R. H. Picard (1998), Mesospheric bores, *J. Geophys. Res., 103(D6)*, 6295–6306.

Dewan, E. M., and R. H. Picard (2001), On the origin of mesospheric bores, *J. Geophys. Res., 106(D3)*, 2921–2928.

Fechine, J., A. F. Medeiros, R. A. Buriti, H. Takahashi, D. Gobbi (2005), Mesospheric Bore events in the Equatorial middle atmosphere, *J. Atmos. Solar-Terr. Phys.*, in press.

Lighthill, J (1978), *Waves in Fluids*, Cambridge Univ. Press, New York.

Mertens, C. J., M. G. Mlynczak, M. Lopez-Puertas, P. P. Wintersteiner, R. H. Picard, J. R. Winick, L. L. Gordley, and J. M. Russell III (2001), Retrieval of mesospheric and lower thermospheric kinetic temperature from measurements of CO_2 15-μm Earth limb emission under non-LTE conditions, *Geophys. Res. Lett., 28*, 1391-1394.

She, C. Y., T. Li, B. P. Williams, T. Yuan, and R. H. Picard (2004), Concurrent OH imager and sodium temperature/wind lidar observation of a mesopause region undular bore event over Fort Collins/Platteville, Colorado, *J. Geophys. Res., 109*, D22107, doi:10.1029/2004JD004742.

Shiokawa, K., Y. Katoh, M. Satoh, M. K. Ejiri, T. Ogawa, T. Nakamura, T. Tsuda, R. H. Wiens (1999), Development of optical mesosphere thermosphere imagers (OMTI), *Earth Planets Space, 51*, 887–896.

Shiokawa, K., Y. Katoh, M. Satoh, M. K. Ejiri, and T. Ogawa (2000), Integrating-sphere calibration of all-sky cameras for nightglow measurements, *Adv. Space Sci., 26*, 1025–1028.

Smith, S. M., M. J. Taylor, G. R. Swenson, C.-Y. She, W. Hocking, J. Baumgardner, and M. Mendillo (2003), A multidiagnostic investigation of the mesospheric bore phenomenon, *J. Geophys. Res., 108(A2)*, 1083, doi:10.1029/2002JA009500.

Shiokawa, K., Y. Otsuka, and T. Ogawa (2005), Quasi-periodic southward-moving waves in 630-nm airglow images in the equatorial thermosphere, *submitted to J. Geophys. Res.,* doi:10.1029/2005JA011406.

Taylor, M. J., D. N. Turnbill, and R. P. Lowe (1995), Spectrometric and imaging measurements of a spectacular gravity wave event observed during the ALOHA-93 campaign, *Geophys. Res. Lett., 22*, 2849–2852.

Zhang, S. P., and G. G. Shepherd (1999), The influence of the diurnal tide on the O(1S) and OH emission rates observed by WINDII on UARS, *Geophys. Res. Lett., 26(4)*, 529–532.

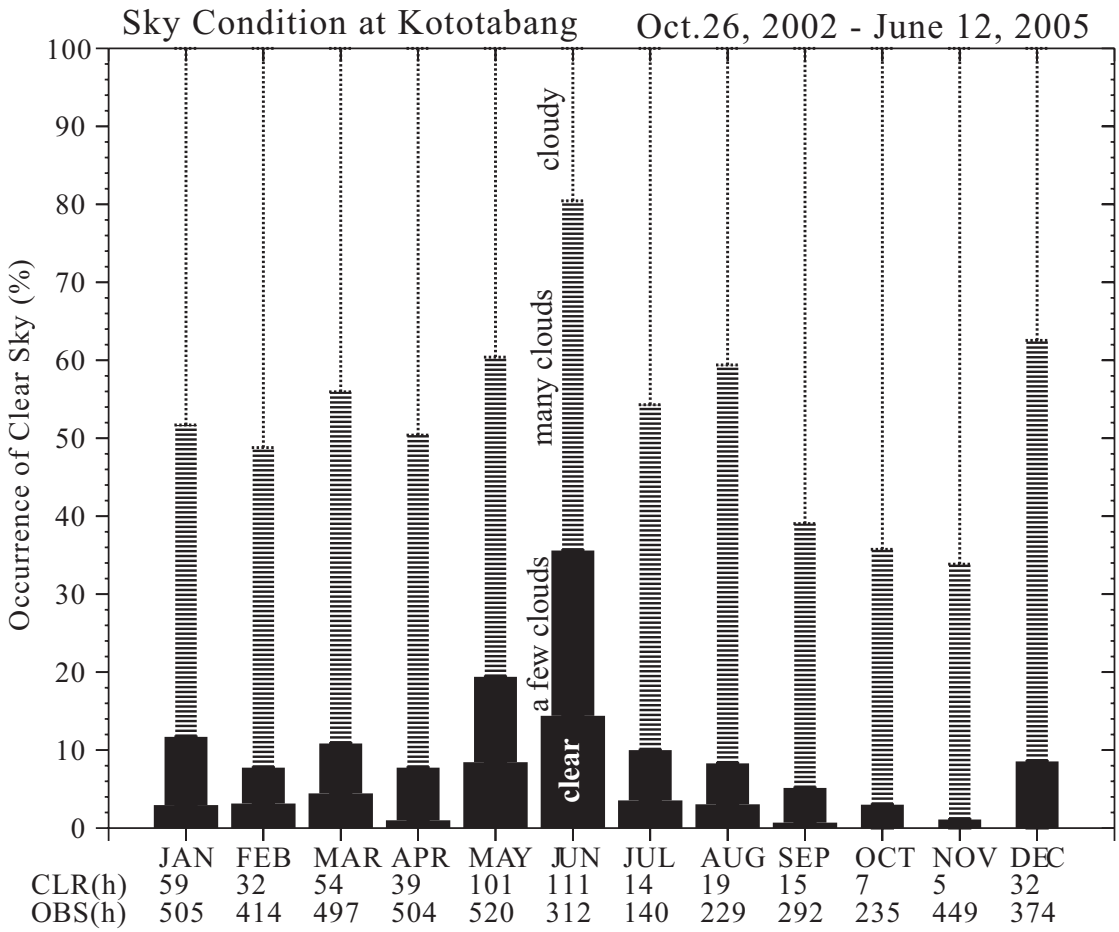

Figure 1. Occurrence of clear sky without clouds at Kototabang, Indonesia, for the period from October 26, 2002 to June 12, 2005. The hourly sky condition is categorized into four classes, i.e., 1. clear with no clouds, 2. clear with a few minor clouds, 3. many clouds with some clear no-cloud parts/intervals, and 4. cloudy. The numbers of hours of clear sky (CLR, 1 and 2) and of observation (OBS) are shown at the bottom of the panel.

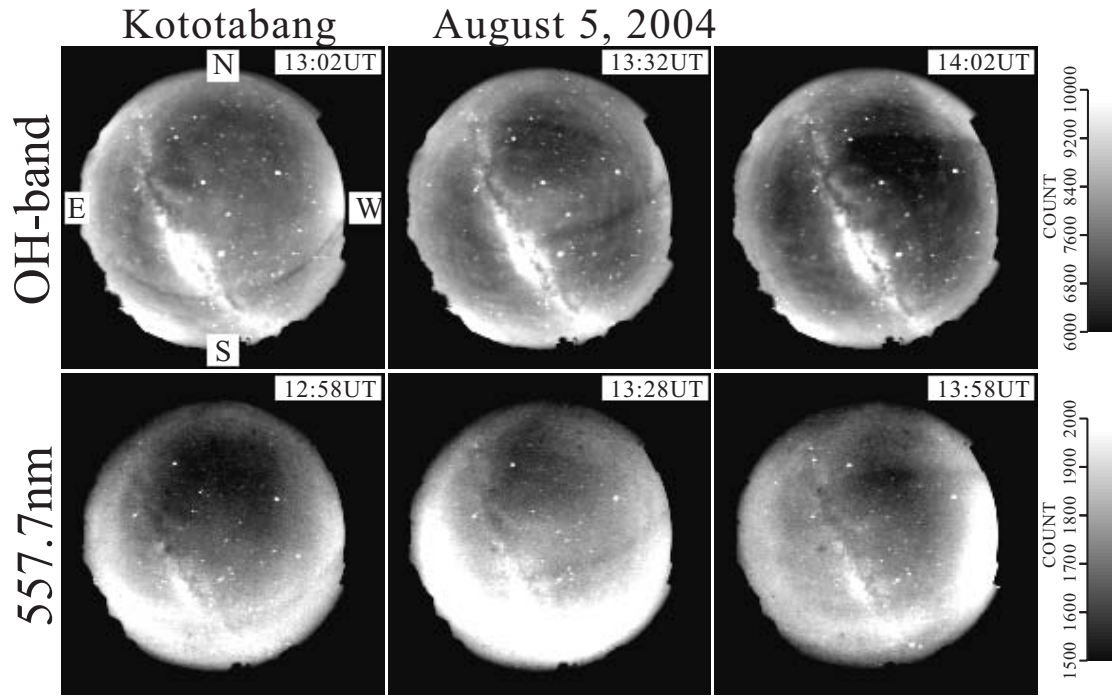

Figure 2. All-sky airglow images of mesospheric bore seen at OH-band (top) and OI (557.7nm) (bottom) at 1258–1402 UT (1958–2102 LT) on August 5, 2004, at Kototabang, Indonesia. The bore can be recognized as east-west dark band moving northward. The bright band from north-east to south in the bottom half of the images is the Milky Way (Galaxy).

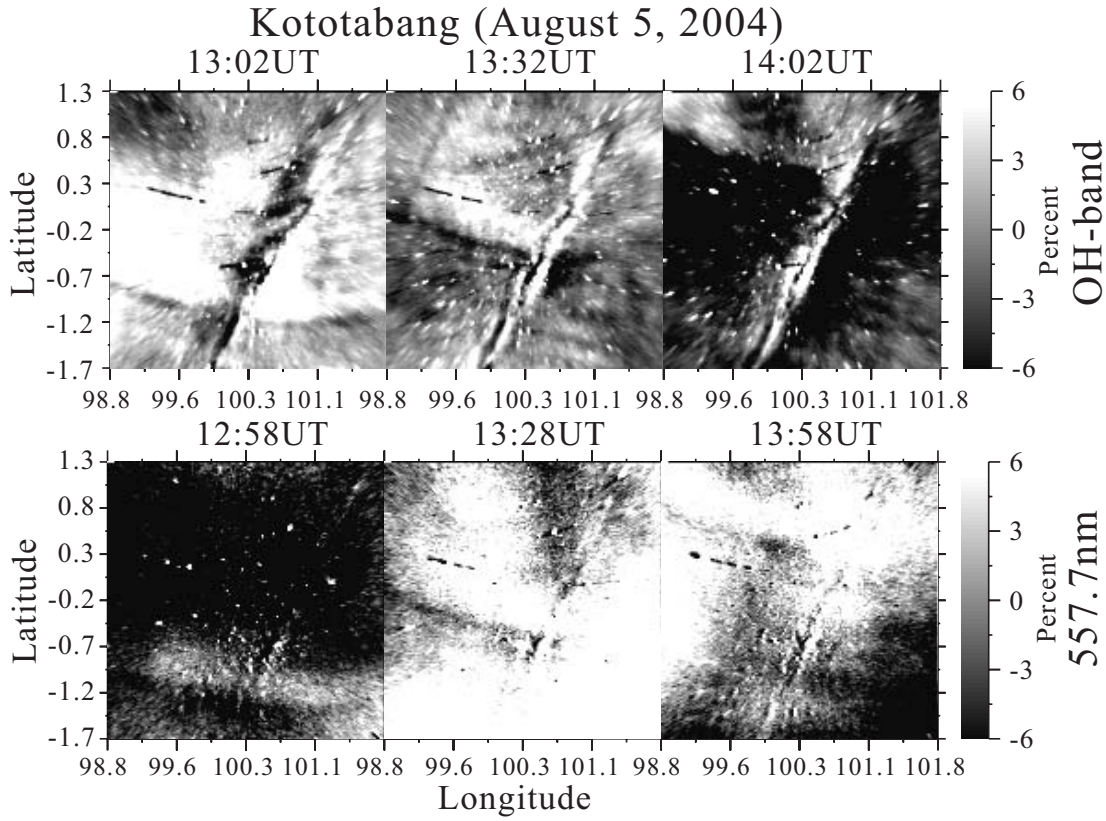

Figure 3. Airglow images of mesospheric bore in geographic coordinates at OH-band (top) and OI (557.7nm) (bottom) on August 5, 2004 at Kototabang, Indonesia. The images are deviations in % from 1.5 hour averages of 1244-1414 UT.

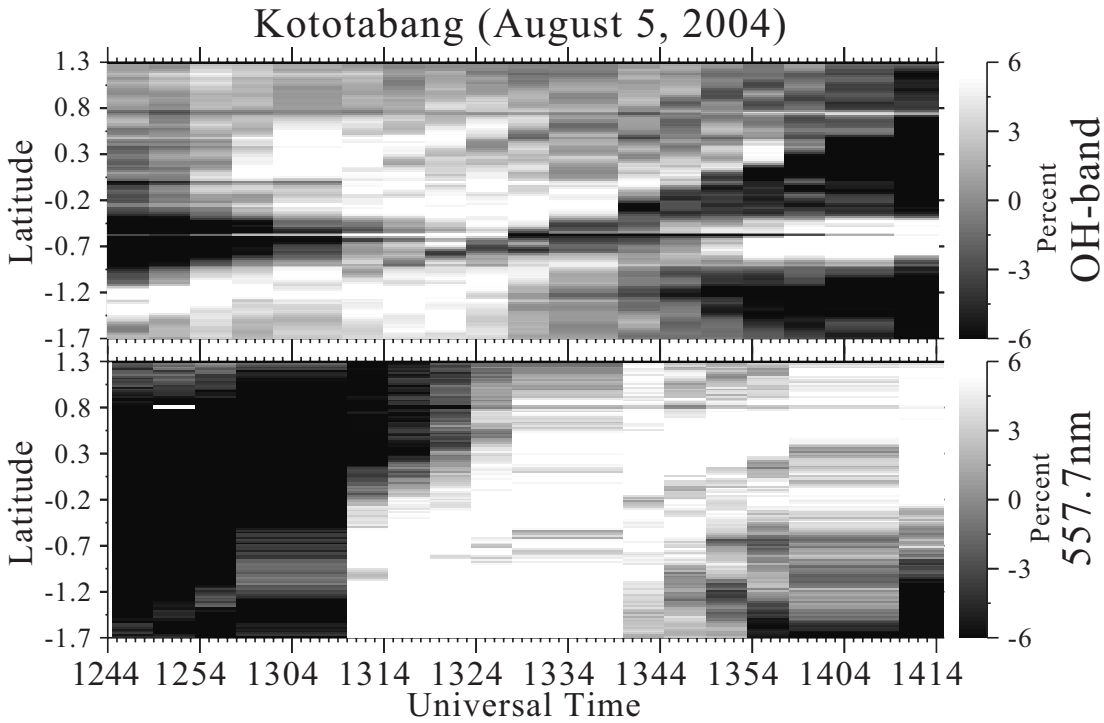

Figure 4. North-south cross sections (keograms) of airglow images in geographic coordinates at OH-band (top) and OI (557.7nm) (bottom) on August 5, 2004 at Kototabang, Indonesia. The data are deviations in % from 1.5 hour averages of 1244-1414 UT. The northward motion of the bore can be seen in both panels.

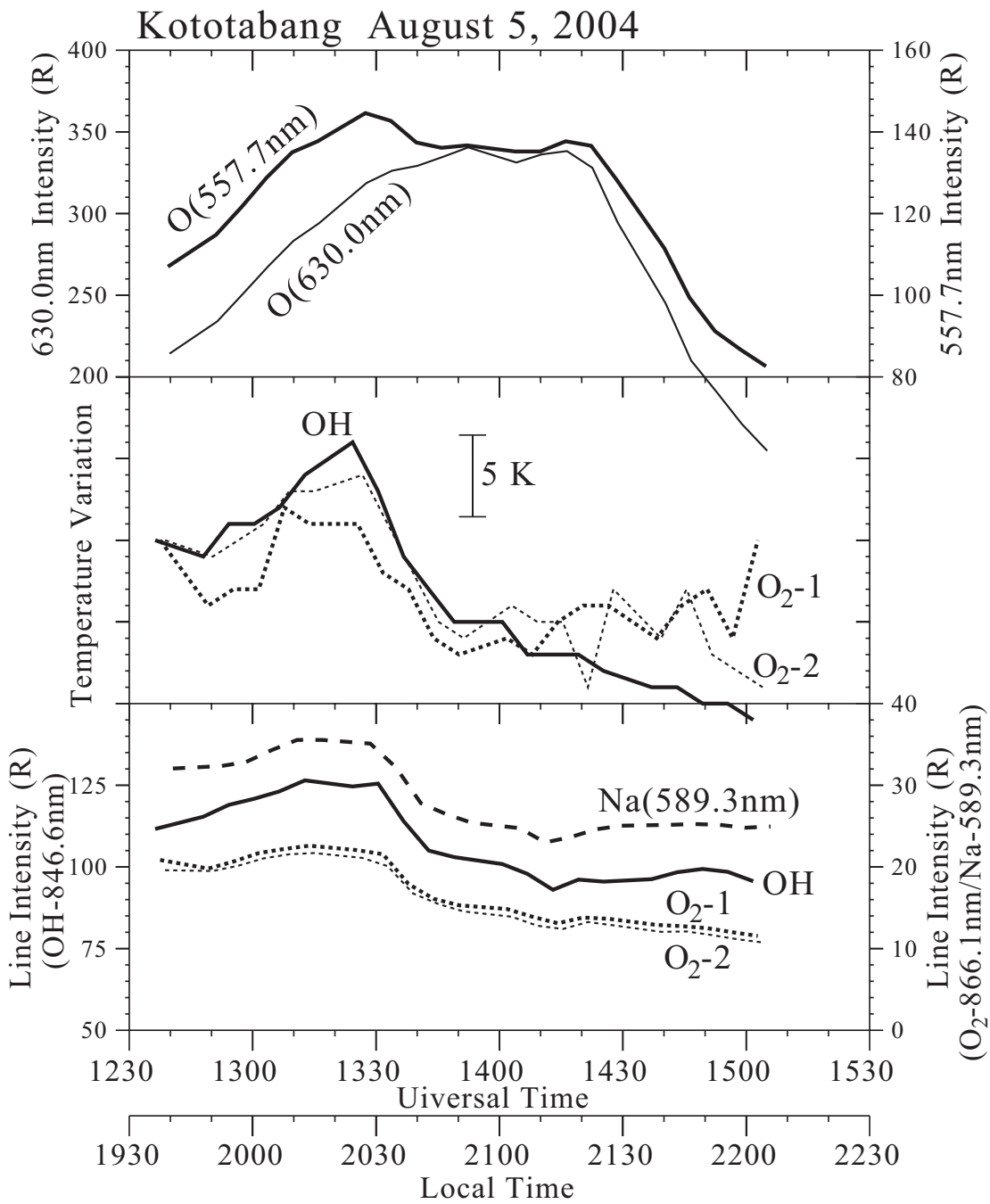

Figure 5. Variations in zenith airglow intensities and rotational temperatures observed by an airglow temperature photometer at Kototabang, Indonesia on August 5, 2004. The mesospheric bore crossed the zenith of Kototabang at ∼1330 UT, when the temperatures and intensities significantly decrease.

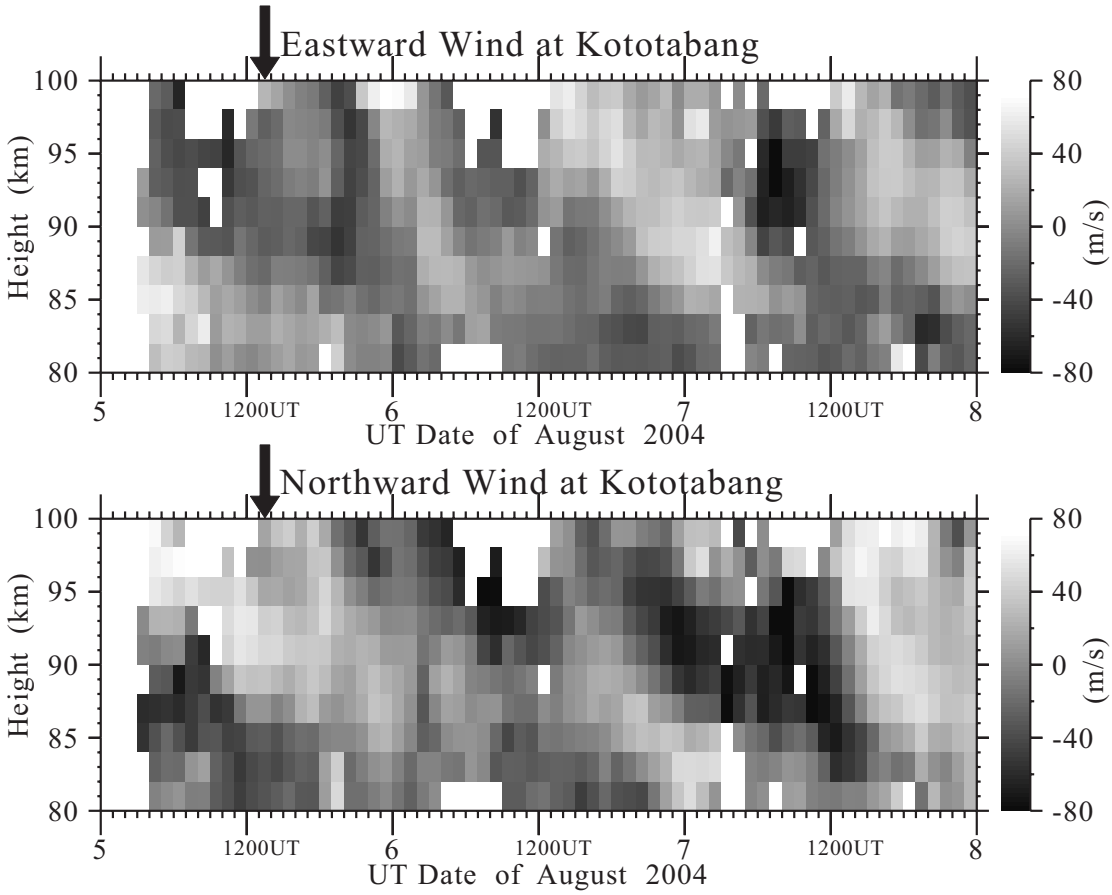

Figure 6. Three-day variations in mesospheric wind measured by a meteor radar at Kototabang, Indonesia, on August 5-7, 2004. The bore was observed in airglow images at 1300-1400 UT, as indicated by the arrows.

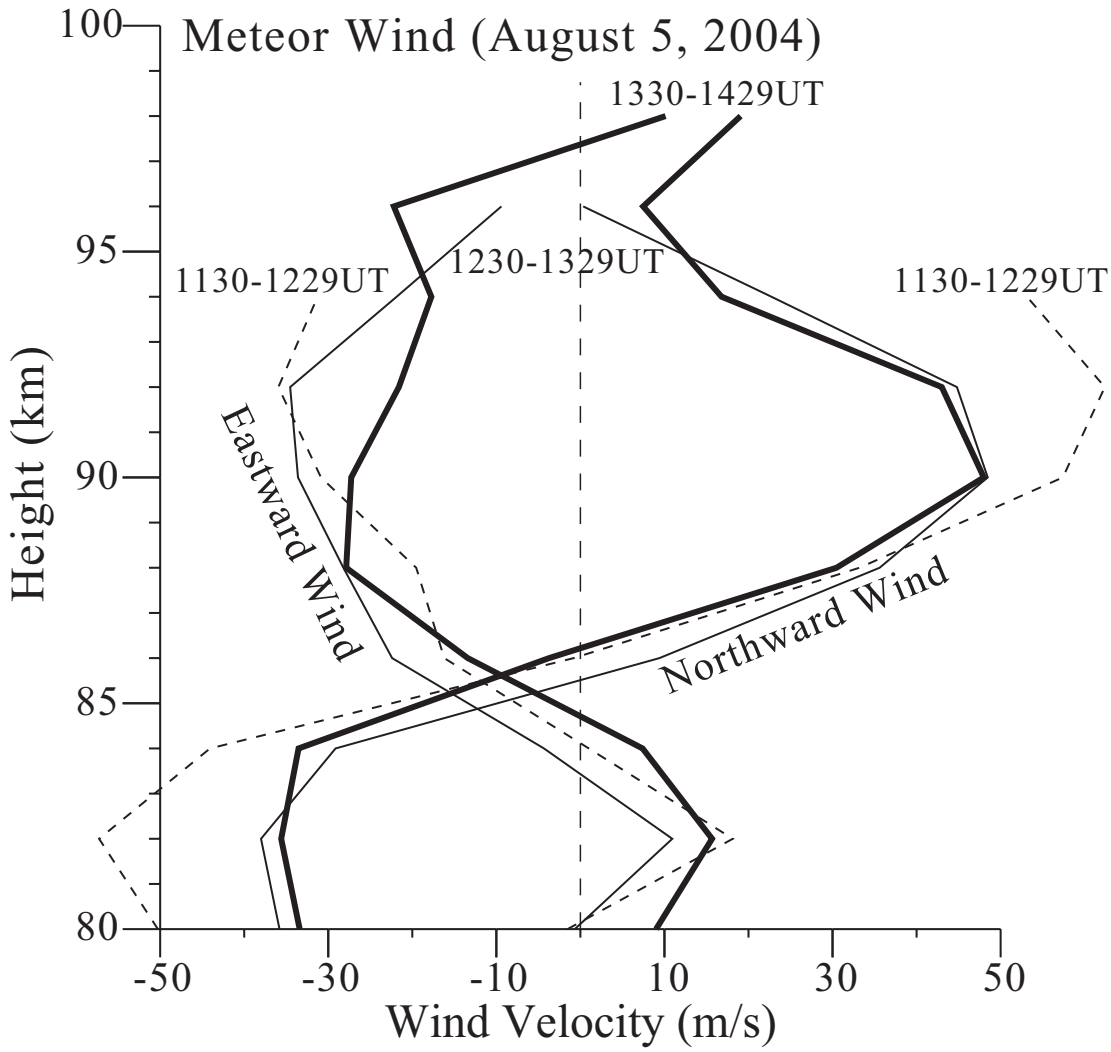

Figure 7. Eastward and northward wind profiles in the mesosphere at three time intervals (1130-1229UT, 1230-1329UT, and 1330-1429UT) measured by a meteor radar at Kototabang, Indonesia, on August 5, 2004.

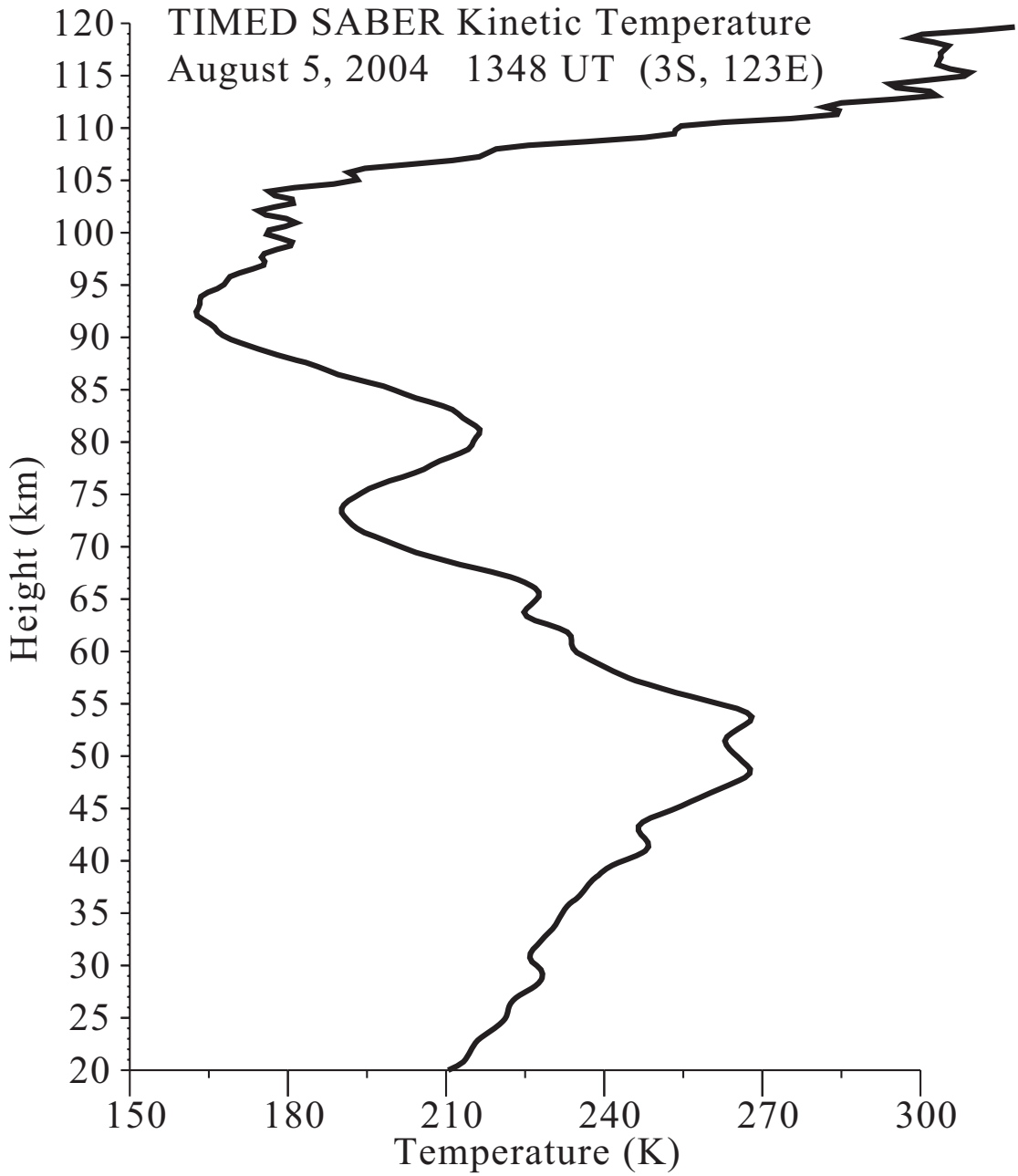

Figure 8. Height profiles of the kinetic temperature measured by the SABER instrument on board the TIMED satellite at 1348 UT on August 5, 2004, at (3°S, 123°E) (∼2500 km east of Kototabang).

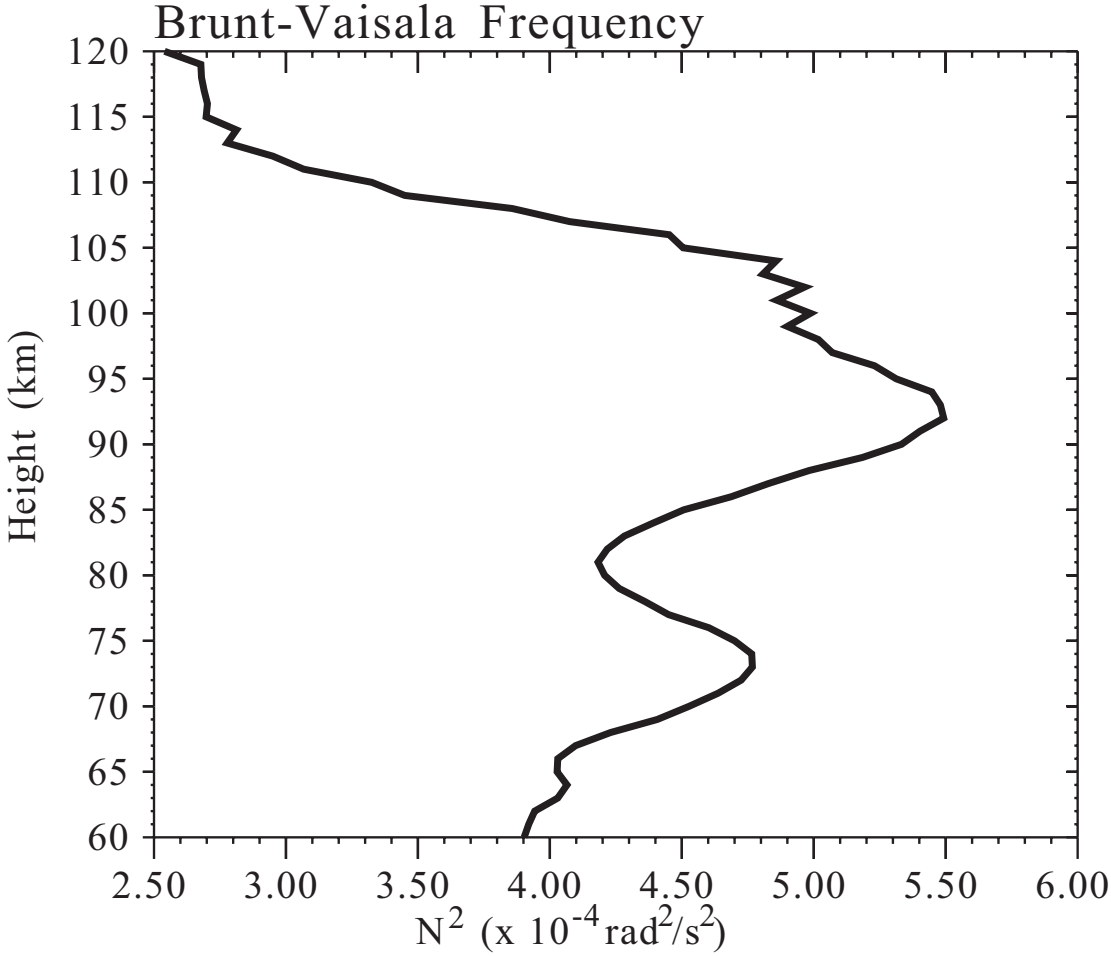

Figure 9. Height profile of the square of the Brunt-Väisälä frequency N^2 calculated from the temperature profile in Figure 8 and the MSIS90 model density profile.